Section 7

Global and regional climate models, sensitivity and impact experiments, response to external forcing, monthly and seasonal forecasting.

Northern Hemisphere snow cover sensitivity to temperature changes in the CMIP6 model ensemble

Arzhanov M.M.[1], Mokhov I.I.[1,2], Parfenova M.R.[1]

[1]A.M. Obukhov Institute of Atmospheric Physics, RAS, 119017, Moscow, Russia
[2]Lomonosov Moscow State University, 119991, Moscow, Russia
arzhanov@ifaran.ru

Estimates of changes in the area of snow cover (SCE) in the Northern Hemisphere in the late 20th - early 21st centuries were obtained using the results of simulations with the ensemble of global climate models CMIP6. Monthly average values of the proportion of snow coverage and surface air temperature of the model grid cells were obtained based on the results of calculations with global climate models (CanESM5, CNRM-ESM2-1, IPSL-CM6A-LR, NorESM2-LM, UKESM1-0-LL) of the international project CMIP6 (https: //esgf-node.llnl.gov/search/cmip6/). For the period 1980-2014, the historical scenario was chosen and for the period 2015-2019, the anthropogenic impacts SSP2-4.5, realization of r1i1p1f1 (in its absence, r1i1p1f2) [1, 2] scenario was used. The SCE used for the calculations for the Northern Hemisphere did not include Greenland SCE.

Figure 1 shows the changes in the SCE depending on the surface air temperature of the Northern Hemisphere for the period 1980-2019 according to calculations with an ensemble of climatic models. The parameter of the sensitivity of the SCE to the changes in the surface air temperature, characterized by the coefficient of the corresponding linear regression, is estimated to be $-3.2(\pm0.1)\times10^6$ km^2 K^{-1}.

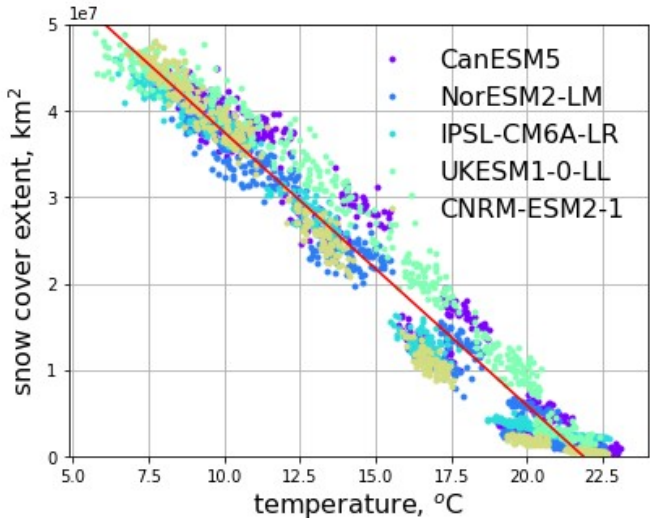

Fig.1. Relationship between the total SCE in the Northern Hemisphere and hemispheric surface air temperature for the period 1980-2019 according to calculations with a climatic models ensemble.

This is close to a similar estimate of the SCE sensitivity parameter to changes in the surface air temperature of -3.6×10^6 km^2 K^{-1} obtained in [3] using the NSIDC (https://www.ncdc.noaa.gov/) and GSL (https://climate.rutgers.edu/) data for the chosen period.

Estimates of changes in SCE in Eurasia and North America for different months depending on the surface air temperature for the two periods 1980-2019 and 2015-2030 are given in Table 1. The highest absolute values were obtained for spring and autumn seasons. The standard deviations

of the regression coefficients are maximum in the autumn period and increase from 1980-2019 period to 2015-2030 period.

Table 1. Values of the linear regression coefficient and standard deviation for the snow cover extent S_s in Eurasia and North America for each month depending on the surface air temperature T_a in Eurasia and North America.

dS_s / dT_a, $\times 10^6$ km^2 / K				
Months	1980–2019		2015-203	
	Eurasia	North America	Eurasia	North America
January	-0.54 (±0.04)	-0.29 (±0.02)	-0.61 (±0.07)	-0.35 (±0.04)
February	-0.63 (±0.04)	-0.29 (±0.02)	-0.67 (±0.08)	-0.40 (±0.05)
March	-0.98 (±0.07)	-0.46 (±0.03)	-1.00 (±0.11)	-0.50 (±0.06)
April	-1.24 (±0.09)	-0.56 (±0.04)	-1.01 (±0.11)	-0.41 (±0.05)
May	-0.99 (±0.07)	-0.52 (±0.04)	-0.58 (±0.07)	-0.18 (±0.02)
June	-1.22 (±0.09)	-0.58 (±0.04)	-0.95 (±0.11)	-0.40 (±0.05)
July	-0.27 (±0.02)	-0.20 (±0.01)	-0.27 (±0.03)	-0.25 (±0.03)
August	-0.40 (±0.03)	-0.24 (±0.02)	-0.39 (±0.04)	-0.16 (±0.02)
September	-1.35 (±0.10)	-0.79 (±0.06)	-1.83 (±0.21)	-0.91 (±0.10)
October	-1.37 (±0.10)	-0.83 (±0.06)	-1.20 (±0.14)	-1.06 (±0.12)
November	-1.09 (±0.08)	-0.72 (±0.05)	-1.36 (±0.15)	-0.92 (±0.10)
December	-0.76 (±0.05)	-0.44 (±0.03)	-0.92 (±0.10)	-0.64 (±0.07)

Linear SCE trend values in the Northern Hemisphere for 1980-2019 according to calculations with an ensemble of models for the winter and spring periods exceed -50×10^3 km^2 yr^{-1}. The results obtained agree well with the estimates obtained in [1]. Analysis of the results of numerical experiments with the ensemble of climate models of the CMIP5 project also showed a decrease in SCE for all seasons for the period 1967–2018. [2].

This work is supported by the Russian Foundation for Basic Research (19-05-00409, 19-35-90118). Regional features of snow cover variability were analyzed within the framework of the Russian Science Foundation project 19-17-00240.

References

[1] Mudryk L., Santolaria-Otin M., Krinner G., Menegos M., Derksen C., Brutel-Vuilmet C., Brady M., Essery R. Historical Northern Hemisphere snow cover trends and projected changes in the CMIP6 multi-model ensemble. *The Cryosphere.* 2020, **14**: 2495-2514.

[2] Connolly R., Connolly M., Soon W., Legates D.R., Cionco R.G., Herrera V.M.V. Northern Hemisphere snow-cover trends (1967–2018): A comparison between climate models and observations. *Geosciences.* 2019, **9** (135): 1-23.

[3] Mokhov I.I., Parfenova M.R. Changes of the sea ice and snow cover extent associated with temperature changes in the Northern and Southern Hemispheres in recent decades. *IOP Conf. Series: Earth and Environmental Science.* 2021. (In press).

Effects of natural GHG emissions under climate changes due to anthropogenic scenarios in the 21st century: Model estimates

Sergey Denisov, Igor Mokhov

A.M. Obukhov Institute of Atmospheric Physics, RAS, Moscow, Russia
denisov@ifaran.ru

An analysis of the ability of natural carbon reservoirs to take up and release carbon requires an adequate account of the carbon balance of boreal forests, wetlands and other ecosystems. We performed simulations with the Earth system model of intermediate complexity developed at the A.M. Obukhov Institute of Atmospheric Physics of Russian Academy of Sciences (IAP RAS CM) to assess the contribution of natural fluxes of carbon dioxide and methane for the major regions of Earth in the 21st century to global climate change under various scenarios of anthropogenic impact. The cumulative influence of the natural CO_2 and CH_4 fluxes to the surface air temperature trends in the 21st century is estimated using the cumulative temperature potential CTP [1] based on global temperature change potential (GTP), which was modified to account for changing background conditions.

The IAP RAS CM belongs to the class of the global climate models of intermediate complexity. It contains modules of the carbon cycle, including partly interactive methane cycle, and a module for calculation of emissions from deforestation and from natural fires. Using the IAP RAS CM, we performed numerical experiments for 1765–2100 with scenarios of anthropogenic impacts on climate due to changes in the content of greenhouse gases in the atmosphere, tropospheric and stratospheric volcanic sulfate aerosols, changes in the total solar irradiance, and changes in the area of agricultural lands. For 1700–2005, these forcings were given in accordance with the "Historical Simulations" of the CMIP5 project. For 2006–2100, the anthropogenic forcings were given prescribed in accordance with the anthropogenic impact scenarios RCP 2.6, 4.5, 6.0 and 8.5.

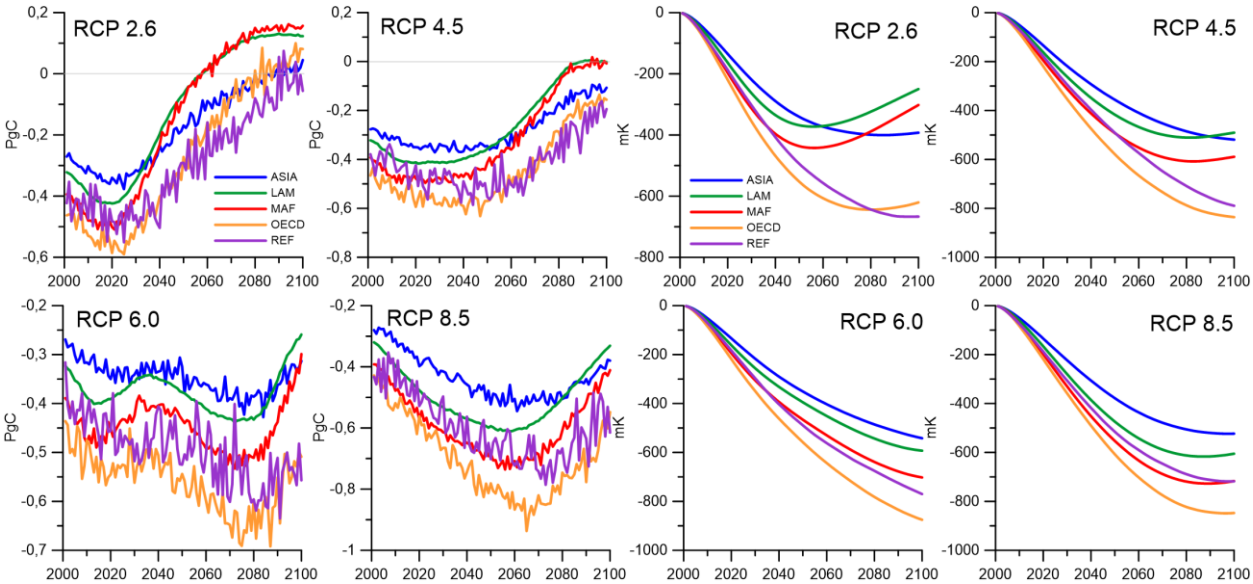

Figure 1. Natural fluxes [PgC] of CO_2 (left) from the RCP regions and their cumulative temperature potential (right).

Cumulative impact on climate was estimated for natural fluxes of CO_2 and CH_4 in the RCP regions, i.e., ASIA (Eastern Asia), MAF (Middle Asia and Africa), LAM (Latin America), OECD (Organization for Economic Co-operation and Development, Western Europe, North America, Australia, Japan), and REF (former USSR, Eastern Europe).

CO_2 uptake (Fig.1) by terrestrial ecosystems for all scenarios and regions considered increases at the beginning of the 21st century. Further in the first (RCP 2.6 and 4.5) or in the second (RCP 6.0 and 8.5) half of the 21st century the maximum absorption is reached after which carbon dioxide uptake begins to decrease. It even switches to emission for LAM and MAF regions under the RCP 2.6 scenario, which can also be observed by the rapid growth of CTP value in the second half of the 21st century. Due to the reduction of CO_2 uptake, the growth of its stabilizing impact on climate slows down noticeably by the

end of the 21st century, except for the RCP 6.0 scenario.

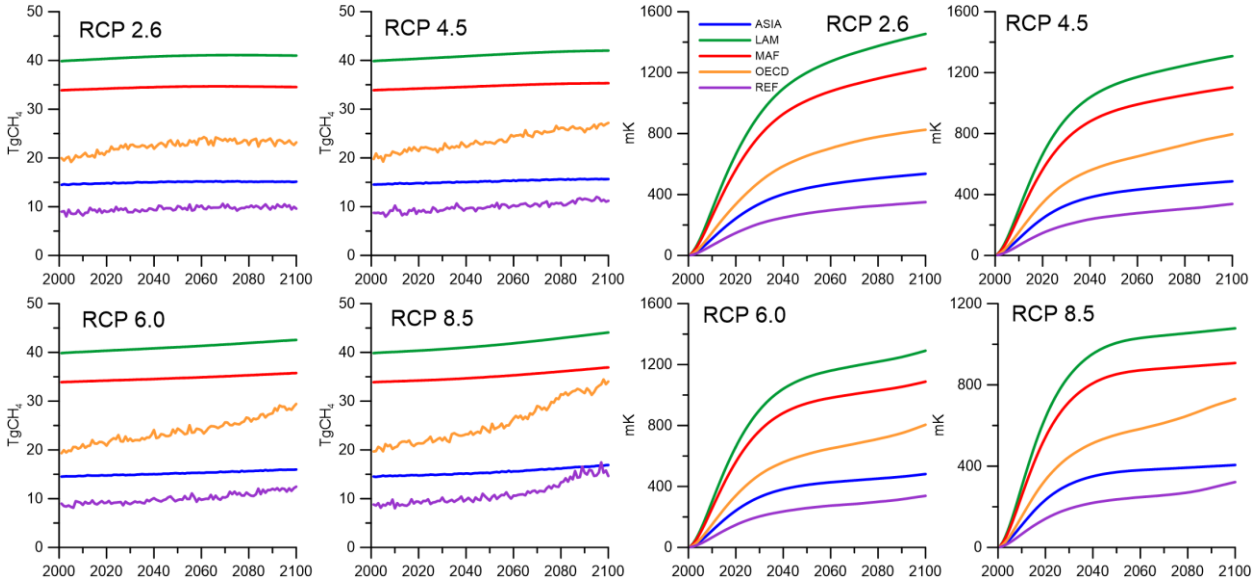

Figure 2. Natural fluxes [$TgCH_4$] of CH_4 (left) from the RCP regions and their cumulative temperature potential (right).

Natural methane emissions from wetlands and the corresponding CTP grow in the 21st century for all scenarios and regions (Fig. 2) due to the growth of the atmospheric temperature. The strongest increase occurs in the OECD and REF regions under the RCP 8.5 scenario where emissions are calculated to double by the end of the century, while in other regions the growth equals to 10-20%. This is due to the fact that in boreal latitudes not only temperature increases faster than average, but also the warm season lengthens.

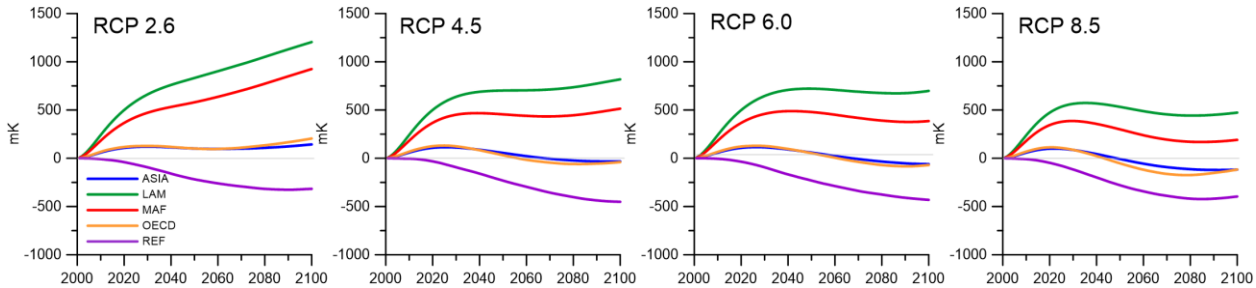

Figure 3. Total natural cumulative temperature potential of the RCP regions.

The total impact of the natural GHG fluxes on global temperature in the 21st century (Fig. 3) clearly supports stabilization of climate only for the REF region. For the ASIA and OECD regions the effects of CO_2 uptake and CH_4 release nearly compensate each other. Relatively high methane emissions from the LAM and MAF regions lead to positive total impact on temperature. The feedback of CO2 flux on higher anthropogenic impact for all regions except REF is stronger than the feedback of CH4 emissions. It leads to lower CTP values for more aggressive anthropogenic scenarios, while for the REF region the total CTP does not differ much between scenarios.

This work was supported by the Russian Foundation for Basic Research (project 19-17-00240).

1. S.N. Denisov, A.V. Eliseev, I.I. Mokhov Contribution of natural and anthropogenic emissions of CO_2 and CH_4 to the atmosphere from the territory of Russia to global climate change in the 21st century // Doklady Earth Sciences. 2019. V.488. N.1. pp. 1066–1071.

Changes of navigation period at the North Sea Route in the 21st century from the CMIP5 ensemble simulations: Bayesian estimates

Eliseev A.V.[1,2], Mokhov I.I.[1,2], Parfenova M.R.[2]

[1]Lomonosov Moscow State University

[2]A.M. Obukhov Institute of Atmospheric Physics RAS

eliseev.alexey.v@gmail.com

A significant decrease in the Arctic sea ice extent during recent decades leads to the increase of navigation period (NP) at the North Sea Route (NSR) (Khon et al., 2010; Khon et al., 2017). Here some estimates of changes in the NP duration on the NSR from the CMIP5 climate models simulations with the use of Bayesian approach (with Bayesian likelihood estimates based on Gaussian distribution) are presented (Kibanova et al., 2018). The analysis used simulations with an ensemble of 25 climate models for the Arctic sea ice concentration under scenarios RCP 4.5 and RCP 8.5 of anthropogenic forcing for the 21st century. Results of simulations were compared with satellite data (obtained from the Scanning Multichannel Microwave Radiometer on the Nimbus-7 satellite) for the period 1980-2018 (Peng et al., 2013). For adequate model estimates of expected changes it is necessary to assess model performance along with multiannual mean and linear trends also interannual variability.

Here are presented the results for the same NSR trajectory as in (Khon et al., 2017). It was assumed that the NSR part was free of ice if its concentration was less than 15%. The NP duration was determined, in particular, for cases where 80 and 90% of the total length of the NSR was free of sea ice. The corresponding analysis was carried out for different parts of the NSR, including the Barents and Kara Seas, the Vilkitsky Channel area, the Laptev and East Siberian Seas.

Figure 1 shows estimates of the NP changes for the Barents and Kara Seas (a) and Laptev and East Siberian Seas (b) from the end of the 20th century based on ensemble model simulations under the RCP 4.5 and RCP 8.5 scenarios for the 21st century in comparison with satellite data.

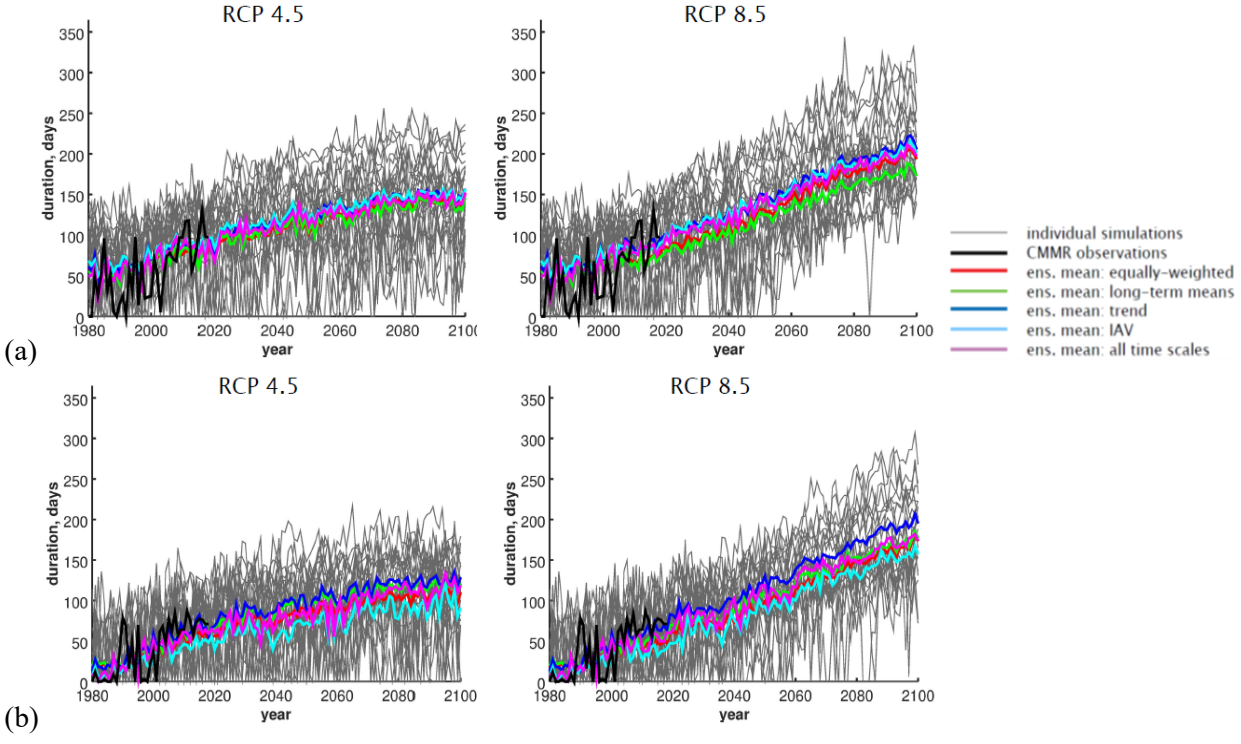

Fig. 1. Ensemble model estimates of changes in NP duration at NSR for the Barents and Kara Seas (a) and Laptev and East Siberian Seas (b) from the end of the 20th century under the RCP 4.5 and RCP 8.5 scenarios for the 21st century in comparison with satellite data.

The ensemble-mean NP duration for the Barents and Kara Seas increases from 55-65 days in 1980-2018 to 138-150 days in 2081-2100 under RCP 4.5 scenario and to 173-204 days under RCP 8.5 scenario depending on Bayesian likelihood choice. The corresponding increase for the Laptev and East-Siberian Seas is from 15-26 days to 94-118 days under RCP 4.5 scenario and to 150-187 days under RCP 8.5 scenario. The largest increase for these two NSR parts, corresponds to the trend-weighted Bayesian estimates, and the smallest increase is produced for the IAV-weighted Bayesian estimates.

It is worth to note that the change of the NP duration in the large NSR parts (Kara and Barents Seas, Laptev and East-Siberian Seas is not too sensitive to the choice of the Bayesian likelihood estimates (except Vilkitsky Channel).

This work was carried out as part of the Russian Science Foundation project 19-17-00240. Analysis of regional features of sea ice variability was supported by Russian Foundation for Basic Research (19-35-90118).

References

Khon V.C., Mokhov I.I., Latif M., Semenov V.A., Park W. (2010) Perspectives of Northern Sea Route and Northwest Passage in the 21st century. *Climatic Change.* **100** (3-4): 757-768.

Khon V.C., Mokhov I.I., Semenov V.A. (2017) Transit navigation through Northern Sea Route from satellite data and CMIP5 simulations. *Environ. Res. Lett.* **12** (2): 024010.

Kibanova O.V., Eliseev A.V., Mokhov I.I., Khon V.C. (2018) Variations in the duration of the navigation period along the Northern Sea Route in the 21st century based on simulations with an ensemble of climatic models: Bayesian estimates. *Doklady Earth Sci.* **481** (1): 909-913.

Peng G., Meier W.N., Scott D.J., Savoie M.H. (2013) A longterm and reproducible passive microwave sea ice concentration data record for climate studies and monitoring. *Earth Syst. Sci. Data*. **5**: 311–318.

About some climatic change in Russia

Vladimir A.Gordin (vagordin@mail.ru)

National Research University Higher School of Economics & Hydrometeorological Centre of Russia, Moscow, Russia.

There is a difference between temperature seasonal plots for various years. To evaluate the long-period change the approximation

$$T(t) \approx S + P\cos(t/L) + R\sin(t/L)\ ,$$

where L = 1 year, may be useful. The first Fourier coefficients S, P, R for a certain year are evaluated by a standard formulae by synoptic station observations in 9 Russian cities separately for the period 2005-2020. The oscillations' amplitude: $A = \sqrt{P^2 + R^2}$ and phase: $\varphi = arctg\left(R/P\right)$ are more informative and visual than the coefficients P, R:

$$T_{jk}(t) \approx S_{jk} - A_{jk}\cos(t/L - \varphi_{jk})\,,$$

where j is the number of year, k is the number of a city.

Let us evaluate by the least squares method (see, e.g. [1]) the temporal tendencies for these cities for a 16-year period. We approximate every function $f\left(j\right) \approx f_0 + f_1 \cdot \left(j - \frac{1+16}{2}\right)$ and obtain

$$S(j,k) \approx S_0(k) + S_1(k)(j-8{,}5);\ A(j,k) \approx A_0(k) + A_1(k)(j-8{,}5);\ \varphi(j,k) \approx \varphi_0(k) + \varphi_1(k)(j-8{,}5),$$

where j = 1,…,16 is the year number. The results are presented in the Table.

We can see that the positive tendencies $A_1(k)$ of the mean temperature are observed for every city (k=1,…,9), although the tendency for Krasnoyarsk is 13 times higher than for Yuzhno-Sakhalinsk. The tendencies $A_1(k)$, $\varphi_1(k)$ are negative for all cities. In other words, the winters become warmer and the seasons begin essentially earlier.

The similar tendencies of the temperature seasonal oscillations for the periods 1936–1965 and 1966–1995 were obtained in [2].

The chronology of the last (before 1 July) frost and the first (after 1 July) frost was evaluated for the cities in the period, too. The essential tendencies are absent and a significant volatility of the days is observed for every city.

Thus, the statement: the Earth's climate is becoming warmer is too simple for the reality description. Its evolution is more complicated.

The use of these tendencies may be important for Russian agriculture, transport, and construction.

Literature

[1] V.A.Gordin. How It Should Be Computed? Computer Assimilation of Meteorological Information. Moscow Center of Mathematical Continuous Education, 2005, 280p. (in Russian). [2] S.M. Semenov, E.S. Gelver. Sine approximation of the annual course of daily mean air temperature in Russia in the twentieth century. Russian Meteorology and Hydrology, 2002, № 11, PP.17-21.

Acknowledgements

The article was prepared within the framework of the Academic Fund Program at the National Research University Higher School of Economics (HSE) in 2020 - 2021 (grant 20-04-021) and by the Russian Academic Excellence Project 5-100.

Table. Temperature tendencies for 9 Russian cities for the period 2005 – 2020.

City	Moscow	Saint Petersburg	Stavropol	Arkhangelsk	Yekaterinburg	Krasnoyarsk	Irkutsk	Khabarovsk	Yuzhno-Sakhalinsk
Index	27612	26063	34949	22550	28440	29570	30758	31735	32150
S_1 C° /year	0.0775	0.068	0.0471	0.0659	0.0276	0.1296	0.105	0.0603	0.0096
A_1 C° /year	-0.112	-0.131	-0.042	-0.122	-0.065	-0.097	-0.137	-0.125	-0.045
φ_1 rad/year	-0.0051	-0.0061	-0.0086	-0.0075	-0.0089	-0.0083	-0.005	-0.0043	-0.0063
φ_1 day/year	-0.30	-0.35	-0.50	-0.44	-0.52	0.48	0.28	0.25	0.37
ΔN_{last} day/year	-0.2	-0.2	-0.1	-0.2	-1	-0,1	0	0.2	-0.2
ΔN_{first} day/year	0.9	-1.2	-0.4	0	-0.1	1.1	1.2	0.2	0.9

Eurasian winter snow variability in the future warming scenarios of CCSM4/CMIP5

Sujata K. Mandke [1,*] and Amita Prabhu[1]

[1] Indian Institute of Tropical Meteorology, Ministry of Earth Sciences, India

*amin@tropmet.res.in, amitaprabhu@tropmet.res.in

1. Introduction

A large fraction of the Eurasian continent is covered with snow during the winter months. Seasonal snow cover over Eurasia is a highly variable component of the global system and has been recognized as an important factor affecting climate variability in the following seasons both locally and in remote regions (Bamzai and Shukla, 1999; Cohen et al. 2012; Wu et al., 2014). The observed trend in the Eurasian snow cover extent (SCE) shows marked seasonal and spatial differences; spring (fall) SCE reveals diminishing (increasing) trend (Yeo et al. 2017). CMIP5 multi-model ensemble confirms widespread reduction of Northern Hemisphere (NH) spring SCE over the 21st century due to climate change, though with considerable inter-model scatter (Collins et al. 2013). In light of the larger sensitivity of NH SCE to climate change (Collins et al. 2013), the present study is focused on the Eurasian winter snow (EWS) variability in a projected future warming, using the 20th century historical and 21st century future projections of three Representative Concentration Pathways (RCP) by the CCSM4 model from the fifth Coupled Model Intercomparison Project (CMIP5; Taylor et al., 2012). The CCSM4 model is chosen due to reasonable simulation of EWS climatology compared to the observation (Prabhu and Mandke, 2019), along with its high horizontal resolution (1.2^{0}E x 0.9^{0}N).

2. Data

Monthly mean snowfall flux data of CCSM4 model for the Reference Period (1850-2005; RP) of the 20th century historical and three RCP scenarios (2.6, 4.5 and 8.5) for the period (2006-2100) of the 21st century from CMIP5 (http://www-pcmdi.llnl.gov), is used.

3. Results

The interannual variability (IAV) (vertical color bars), trend (dashed black line) overlaid by the decadal variability (color shading) of winter snowfall flux averaged over Eurasian region (50- 70°N; 20-140°E) in historical and three RCP simulations of CCSM4 model from CMIP5 are depicted in Figures 1a, 1b, 1c, and 1d respectively. The averaged conditions from December through March of the following year (DJFM) are chosen as representative of the winter season due to prevalence of maximum snow over Eurasia during DJFM in the annual cycle (Prabhu and Mandke, 2019). The target Eurasian region is selected because it is one of the main snow cover areas and also winter/spring snow over this region exert strong influence on the All-India summer monsoon rainfall (Yim et al., 2010). A trend of EWS in historical and three RCPs is declining with the largest downward trend in RCP8.5 and a relatively very weak trend in RCP2.6. IAV of EWS during RP is dominated by positive (negative) anomalies before (after) 1970's. This results in prevalence of weak positive (strong negative) conditions before (after) 1970s in the decadal variability of EWS during RP. The EWS variability (IAV and decadal) in RCP2.6 do not agree with RCP4.5 and RCP8.5 with regard to timing of the positive/negative anomalies. The time series of EWS in RCP4.5 displays similarity in its long-term behavior to RCP8.6, although the amplitude of anomalies (IAV and decadal) is higher in RCP8.6. The decadal variability of EWS in RCP2.6 is characterized by positive anomalies from 2006 till early 2030s and later near normal or negative conditions, still its amplitude is small. The positive phase of decadal variability persisted from 2006 till mid-2050s and thereafter is negative in both RCP4.5 and RCP8.6. As the results of the present study are based on the simulations of a single model, detailed analysis with CMIP6 multi-model ensemble future climate change simulations would provide possible extension of this work.

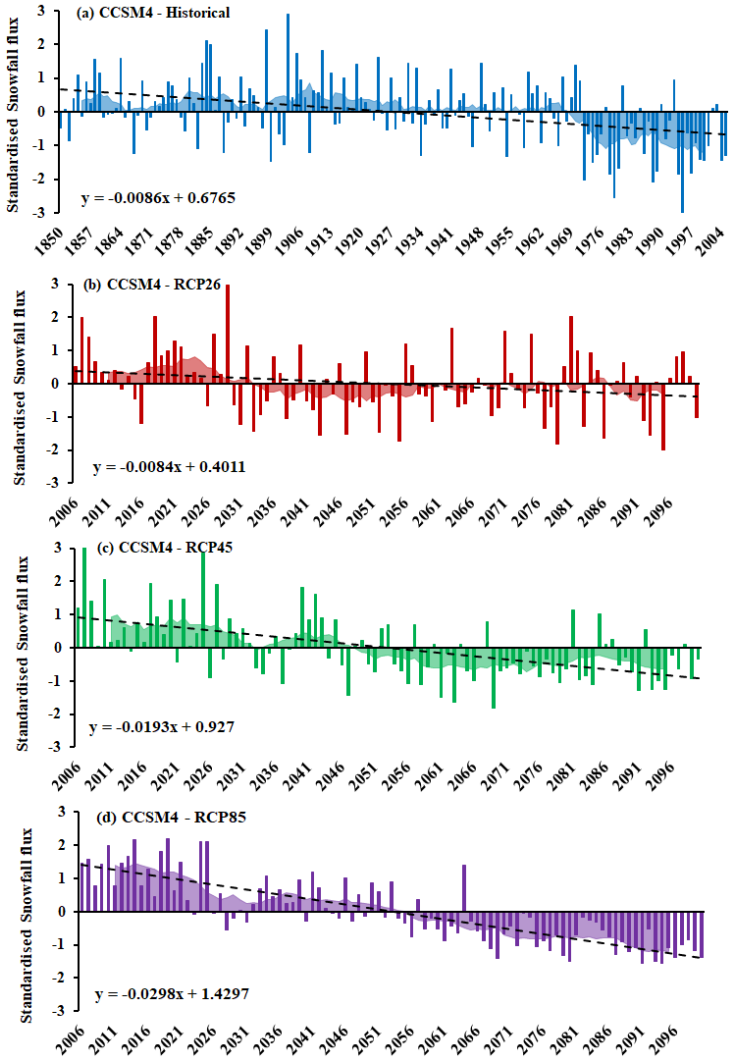

Figure 1: Variability of winter snow averaged over Eurasia (50-70°N, 20-140°E) simulated by CCSM4/CMIP5 model. Vertical color bars (year-to-year variations); Color shading (decadal variability); Black dashed line (trend) (a) Historical run (b) RCP2.6 (c) RCP4.5 (d) RCP8.5

References: Bamzai A. S., and J. Shukla, 1999. Relation between Eurasian snow cover, snow depth, and the Indian summer monsoon: An observational study. J. Climate, 12, 3117–3132.

Cohen, J. L. and coauthors. 2012. Arctic warming, increasing snow cover and widespread boreal winter cooling. Environ. Res. Lett., 7(1).

Collins, M. and co-authors, 2013. Long-term Climate Change: Projections, Commitments and Irreversibility, Climate Change 2013 - The Physical Science Basis: Contribution of Working Group I to the 5th Assessment Report of the IPCC, 1029-1136.

Prabhu, Amita and Mandke, Sujata, 2019. Indian rainfall and Eurasian snow climatology in CMIP5 historical simulations. Research activities in atmospheric and oceanic modeling, CAS/JSC Working Group on Numerical Experimentation. Report No. 49. WCRP Report No.12/2019. WMO, Geneva p. 9-03.

Taylor K.E., Stouffer R.J. and Meehl G.A., 2012. An overview of CMIP5 and the experiment design, Bull. Amer. Meteorol. Soc, 90(4) :485–498.

Wu, R., Liu, G. and Ping, Z. 2014: Contrasting Eurasian spring and summer climate anomalies associated with western and eastern Eurasian spring snow cover changes. J. Geophys. Res. Atmos., 119, 7410–7424.

Yeo, S. R., Kim, WM, Kim, K. Y., 2017. Eurasian snow cover variability in relation to warming trend and Arctic Oscillation. Clm Dyn, 48, 499-511.

Yim, S.-Y., J.-G. Jhun, R. Lu, and B. Wang, 2010: Two distinct patterns of spring Eurasian snow cover anomaly and their impacts on the East Asian summer monsoon. J. Geophys. Res., 115, D22113.

Atmospheric centers of action in the Northern and Southern Hemispheres: Tendencies of change in the 21st century from model simulations

Mokhov I.I.[1,2], Chernokulsky A.V.[1], Osipov A.M.[2]

[1]A.M. Obukhov Institute of Atmospheric Physics RAS

[2]Lomonosov Moscow State University

mokhov@ifaran.ru

The key large-scale structures in the atmosphere of the Earth climate system are atmospheric centers of action (CoA). CoA are clearly manifested in monthly and seasonal distributions of surface air pressure and characterize features of general atmospheric circulation [1,2]. Here, we estimate possible changes of CoA associated with global climate changes using simulations with the CMIP5 ensemble of climate models under various RCP scenarios of anthropogenic forcing in the 21st century, including the RCP4.5 and RCP8.5 scenarios.

Table 1 presents the estimates of changes in the intensity of various CoA by the end of the 21st century from simulations of monthly-mean surface pressure with INM-CM4, IPSL-CM5A-MR, MPI-ESM-MR climate models under the scenario RCP4.5. The CoA intensity was characterized by the extremal surface pressure Pextr and mean surface pressure Pmean for the corresponding CoA region (see [1,2]). Table 1 shows changes in the intensity of CoA (in hPa) for the period 2070–2099 relative to 1976–2005 in winter and summer.

Table. Changes in the intensity of CoA (hPa) for the period 2070-2099 relative to 1976–2005 in different seasons from simulations with three climate models under the RCP4.5 scenario with moderate anthropogenic forcing in the 21st century. Statistically significant changes at the 0.1, 0.05, and 0.01 significance levels are shown in italic, bold italic, and bold type, respectively. The blue color characterizes the strengthening (deepening) of the lows, red color shows the strengthening of the highs, the green color displays the weakening of the CoA.

CoA	INM-CM4		IPSL-CM5A-MR		MPI-ESM-MR	
	P mean	P extr	P mean	P extr	P mean	P extr
Southern Hemisphere						
Winter (June-August)						
Minima						
Indian	**-1.7**	**-1.5**	**-3.1**	**-2.7**	**-2.1**	**-2.1**
South Atlantic	**-0.9**	***-0.8***	**-2.6**	**-2.0**	**-2.2**	**-2.3**
South Pacific	***-1.0***	***-1.0***	**-3.0**	**-3.6**	*0.6*	**-2.0**
Maxima						
Antarctic	**-2.5**	**-2.8**	**-6.1**	**-6.2**	**-2.6**	**-2.8**
Mascarene	0.3	0.4	**1.2**	**1.2**	**0.8**	*0.5*
South Atlantic	0.3	0.3	0.3	0.3	***0.6***	**0.9**
South Pacific	**0.7**	**0.7**	**1.5**	**1.2**	*0.6*	***0.6***
Summer (December-February)						
Minima						
Indian	0.0	0.3	**-1.6**	**-1.4**	**-1.4**	**-1.4**
South Atlantic	0.0	0.2	**-2.1**	**-1.9**	**-1.5**	**-1.6**
South Pacific	0.5	*0.7*	**-4.7**	**-4.4**	**-2.0**	**-1.9**
Maxima						
Antarctic	-0.6	***-0.9***	**-7.3**	**-7.2**	**-2.8**	**-2.9**
Mascarene	-0.1	0.0	***0.5***	**0.7**	0.3	0.4
South Atlantic	0.0	0.0	***0.5***	***0.5***	0.1	0.2
South Pacific	-0.1	0.0	**0.9**	**0.6**	0.3	0.2

CoA	INM-CM4		IPSL-CM5A-MR		MPI-ESM-MR	
	P mean	P extr	P mean	P extr	P mean	P extr
Northern Hemisphere						
Winter (December-February)						
Minima						
Aleutian	***-0.8***	**-1.2**	-0.5	0.1	-0.4	*-0.7*
Islandic	**-1.7**	**-2.1**	*-0.9*	*-1.0*	-0.5	*-0.9*
Maxima						
Azores	***0.6***	**1.0**	-0.3	-0.4	*0.5*	***0.8***
Arctic	**-1.7**	**-1.8**	**-2.2**	**-2.7**	**-2.0**	**-1.9**
North Pacific	-0.5	0.1	0.1	***-0.7***	0.4	0.0
Greenland	**-1.9**	**-1.7**	0.0	0.5	***-1.2***	-0.8
North American	***-0.7***	*-0.6*	***-0.8***	-0.6	***-0.6***	-0.4
Siberian	*-0.5*	***-0.7***	***-0.7***	**-1.3**	*-0.6*	-0.4
Summer (June-August)						
Minima						
Asian	**-0.6**	**-0.7**	**-0.6**	***-0.4***	-0.1	0.0
Aleutian	**0.6**	-0.1	***-0.5***	*-0.4*	***-0.6***	***-0.5***
Islandic	**-0.9**	**-1.3**	**-1.2**	**-1.0**	0.3	0.2
	0.0	-0.1	***-0.4***	**-0.5**	**0.9**	**0.9**
Maxima						
Azores	-0.2	*0.4*	**-0.6**	0.0	0.1	0.3
Arctic	-0.4	-0.3	**-1.1**	**-1.6**	-0.1	-0.2
North Pacific	***0.3***	**0.5**	*-0.4*	0.1	-0.3	-0.4
Greenland	**-1.0**	***-0.9***	**-1.9**	**-2.6**	-0.3	-0.5

Results of model simulations in Table 1 under the RCP 4.5 scenario show general strengthening (deepening) of cyclonic CoAs (both year-round and seasonal) in both hemispheres for the last 30 years of the 21st century, relative to the current regime (1976–2005). At the same time, different trends appear for the North American summer minimum (low) for different models. For anticyclonic CoAs in the Northern Hemisphere, a general weakening of winter continental CoA prevails, the development of which is associated with surface cooling in the cold season. The most significant weakening was noted for the Greenland High. An increase in the intensity (stronger in winter) of oceanic subtropical maxima (highs), in particular in the Southern Hemisphere, can be associated with the expansion of the Hadley cell during global warming. In the Northern Hemisphere, for different models, differently directed tendencies of changes for the Azores and Hawaiian maxima (highs) were revealed. Weakening of the polar highs (Arctic and Antarctic) is noted, which is more pronounced in winter. This is associated with the poleward shift of the trajectories of extratropical cyclones. A more significant weakening is manifested under the RCP-8.5 scenario with stronger anthropogenic forcing in the 21st century.

This work was supported by the Russian Science Foundation project 19-17-00240.

References

[1] Mokhov I.I., Chernokulsky A.V., Osipov A.M. Changes in the characteristics of atmospheric centers of action. In: *Intense Atmospheric Vortices and Their Dynamics.* Ed. By I.I. Mokhov, M.V. Kurgansky, O.G. Chkhetiani. Moscow, GEOS, 482 pp. (In Russian)

[2] Mokhov I.I., Chernokulsky A.V., Osipov A.M. Atmospheric centers of action in the Northern and Southern Hemispheres: Features and variability. *Russ. Meteorol. Hydrol.*, 2020, **45** (10): 749-761.

Influence of climate system nonlinearity on the time lag between changes in global temperature and atmospheric CO_2 content

Muryshev K.E.[1], Eliseev A.V.[1,2], Mokhov I.I.[1,2], Denisov S.N.[1], Arzhanov M.M.[1], Timazhev A.V.[1], Narizhnaya A.I.[1]

[1]A.M. Obukhov Institute of Atmospheric Physics RAS

[2]Lomonosov Moscow State University

kmuryshev@mail.ru

The numerical simulations with IAP RAS climatic model (IAP RAS CM) under idealized scenarios of external forcing for the Earth system are performed. The external forcings include anthropogenic emissions of CO_2 into the atmosphere $E_{CO2}(t)$ and variations of the solar constant $F(t)$. The following scenarios of external influences are used:

1. Greenhouse	$F = 0$	$E_{CO2} = E_{CO2,A} \sin(\omega t)$
2. Non-greenhouse	$F = F_A \sin(\omega t)$	$E_{CO2} = 0$

Here $E_{CO2,A}$ and F_A are the amplitudes of the forcing, ω – is the frequency of the forcing. The simulations were performed with external forcings at the time scales $P = 2\pi/\omega$ from 10 to 2000 years with amplitudes of emissions $E_{CO2,A} = \{1, 2, 5, 10\}$ GtC/yr, the amplitudes of variations of the solar constant $F_A = \{6.825, 13.65, 27.3\}$ W/m^2 corresponding to its deviations by 0.5, 1 and 2 % from the current value of 1365 W/m^2.

The time lag Δ between the series of global temperature T and atmospheric CO_2 content q obtained in these numerical experiments was investigated.

It was previously shown that the sign of Δ depends on the type of external forcing and its time scale [1-3]. In this work, it was found that when Δ is calculated using narrow time intervals (of the order of $P/2$), its sign depends on whether T and q increase or decrease over these intervals, as well as on the amplitude of their variations. When the amplitudes of T and q variations are large enough, the response of one variable to changes in the other is markedly different from the linear one. The dependence of T on changes in q is close to logarithmic, and the dependence of q on changes in T is exponential.

As a result, if the variations of T and q are approximately in-phase, then at the growth stage T is leading q, and at the decreasing stage q is leading T, regardless of the type of external forcing, greenhouse or non-greenhouse (see Figure 1).

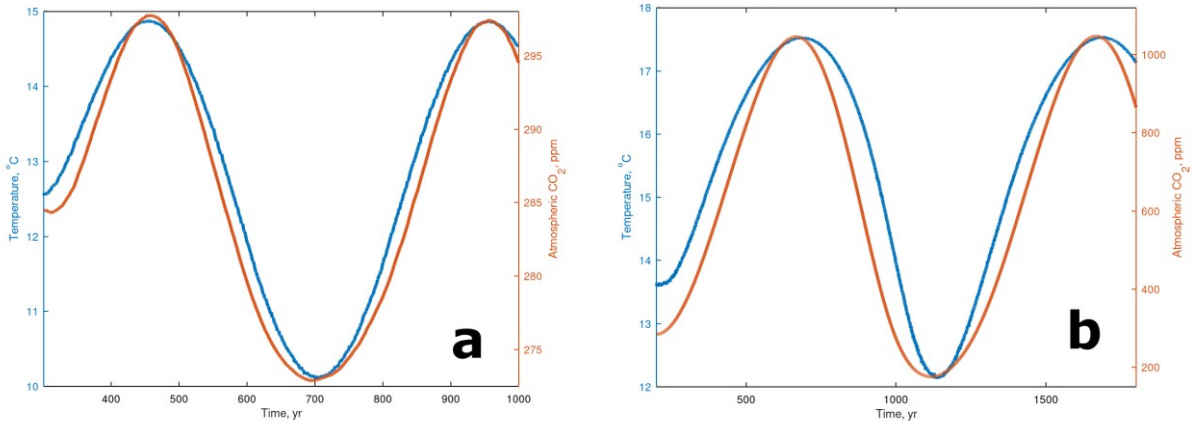

Fig. 1. Changes in global temperature T (blue curve) and atmospheric CO_2 concentration q (orange curve) in the numerical simulations with IAP RAS CM under non-greenhouse external forcing with P = 500 yr and F_A = 27.3 W/m^2 (a) and greenhouse forcing with P = 1000 yr and $E_{CO2,A}$ = 10 GtC/yr (b).

For small amplitudes of T and q variations, their response to each other's changes is close to linear, so the sign of Δ does not depend on the increase or decrease of the variables over the considered time interval.

This study was supported by the Russian Science Foundation (project no. 19-17-00240).

References

1. Muryshev K.E., Eliseev A.V., Mokhov I.I., Timazhev A.V. A lag between temperature and atmospheric CO_2 concentration based on a simple coupled model of climate and the carbon cycle. *Doklady Earth Sciences,* 2015, V. 463, Part 2, P. 863-867
2. Muryshev K.E., Eliseev A.V., Mokhov I.I., Timazhev A.V. Lead-lag relationships between global mean temperature and and the atmospheric CO_2 content in dependence of the type and time scale of the forcing. *Global and Planetary Change,* 2017, V. 148, P. 29–41.
3. Muryshev K.E., Eliseev A.V., Denisov S.N., Mokhov I.I., Arzhanov M.M., Timazhev A.V. Phase Shift between changes in global temperature and atmospheric CO2 content under external emissions of greenhouse gases into the atmosphere. *Izvestiya, Atmos. Ocean. Phys.*, 2019, V. 55, P. 235–241.